CLAS-Note 2003-012

Kinematics Corrections for CLAS

Kijun Park, Volker Burkert, Latifa Elouadrhiri, Wooyoung Kim
Kyungpook National University, Daegu, Korea 702-701
Jefferson Lab, 12000 Jefferson Avenue, Newport News, VA 23606

August 11, 2003

Abstract

We discuss kinematics corrections to the CLAS event reconstruction that are needed to correct for our incomplete knowledge of the CLAS detector geometry and magnetic field distribution. We develop simple corrections using the kinematic constraints from overdetermined reactions, elastic scattering $ep \to ep$, and π^+ production $ep \to e\pi^+ n$. Angle corrections and momentum corrections are determined independent of each other. We test the resulting corrections on various exclusive processes, e.g. $ep \to ep\pi^\circ$, $ep \to ep\eta$, $ep \to ep\omega$, and find significant improvements in mass position and resolution.

1 INTRODUCTION

The problem of kinematics corrections for CLAS is as old as when the CLAS electron scattering events were reconstructed. These were first discussed initially in a CALCOM meeting [1] during the commissioning phase and during the early data taking phase of CLAS. The evidence for the need of such corrections is most directly seen in the dependence of the elastic peak position on the azimuthal angle of the reconstructed electrons, as shown in Figure 1. If the kinematics remains uncorrected, the physics processes of interest, e.g. $ep \to ep\pi^\circ$, $ep \to ep\eta$, $ep \to en\pi^+$, $ep \to ep\omega$, $ep \to ep\pi^+\pi^-$, show wider than expected mass distributions located at slightly shifted masses. This influences our capabilities to separate signal from background, and has most undesirable effects on the determination of physics quantities, such

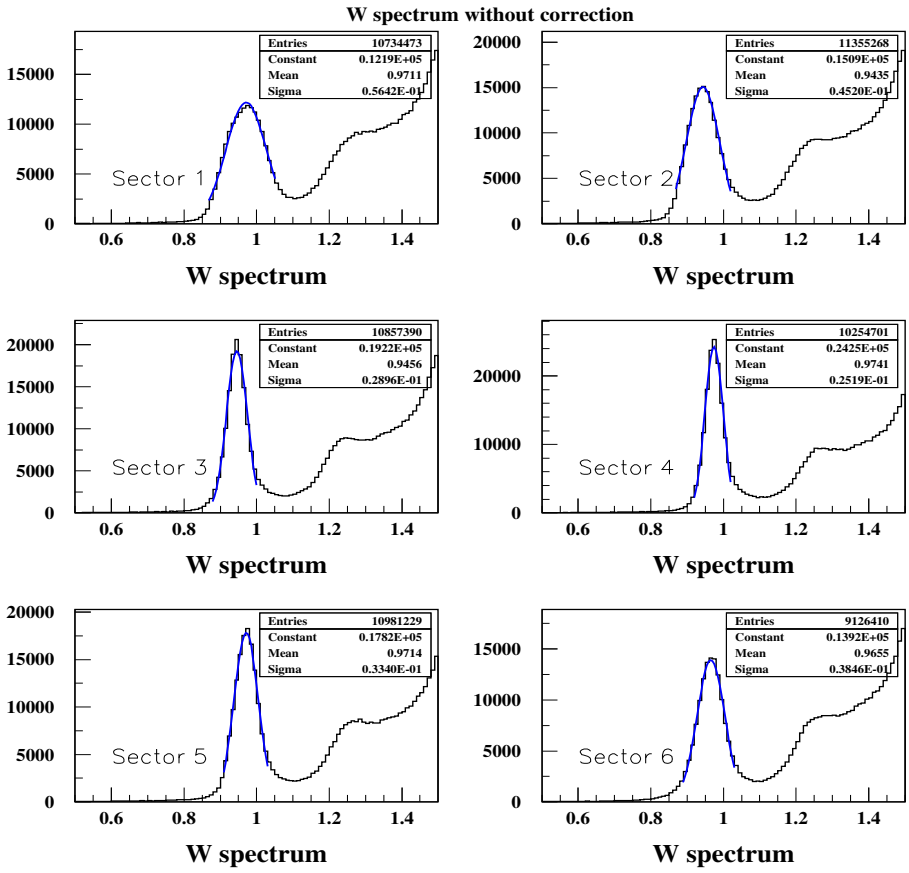

Figure 1: The missing mass distribution W in $ep \rightarrow eX$ for all six sectors. The sector dependence of the elastic peak position and the peak width are clearly seen. From left top to right bottom, from sector 1 to 6

as energy-dependence of partial waves, etc. from such processes. Since the effects are of unknown origin, they cannot be simulated in GSIM. This makes it mandatory to have, at the very least, first order corrections to the 3-momentum vectors determined in track reconstruction. In our approach we try to go beyond the first order corrections without attempting to develop a global procedure to develop corrections for the entire phase space. Such a procedure is justified, as we will demonstrate by comparing our results with a much simpler appraoch, resulting in similar results.

2 Data sets used

We used the E1-6 full data sets to correct the angle and momentum of negative charged particle (e^-) and positive charged particle (π^+). E1-6 data contained only one set of experimental condition with one beam energy ($E_0 = 5.754GeV$) and magnetic field setting ($I_B = 3375.0A$). We used the reduced ntuples which contain a minimum number ntuple variables. This saved time during the correction procedure.

3 Description of Method

3.1 Assumptions

In order to keep the problem tracktable we have made several assumptions which we feel are reasonable. We will provide some arguments why this may be the case.

Assumption 1 *As a first assumption we equate the beam energy to the energy as measured by the Hall A procedures (elastic ep scattering and energy measurements in the arcs. Both measurements agree within less than 6 MeV [3] for the 5.754 GeV run.*

Assumption 2 *We further extract all corrections from one data run (e1-6) with fixed beam energy and fixed torus current of $I_{torus} = 3375$ A. We determine the correction for other torus currents simply by scaling the particle momenta and torus current. This can only be approximately correct, as the mini-torus current remains fixed at 6000 A, while only the torus current is usually changed. The mini-torus current provides only about 5% of the $\int Bdl$ of the full torus magnetic field. We therefore argue that the effect of the mini-torus field on the particle trajectories is small. And since the corrections are of the order of O(1%) in momentum, and O(1 mrad) on polar angle, the effect of the mini-torus is expected to be much smaller than these.*

Assumption 3 *Our main assumption is that the particle's polar angle are reconstructed correctly for scattering angles greater than 35 degrees. Although one could bring arguments why this should be the case, we prefer to justify this assumption by the results.*

Assumption 4 *In addition, we assume that the angle corrections are independent of the particle's charge.*

3.2 Angle corrections

3.2.1 Procedure

Following the suggestion by Cole Smith [2], we separate the angle corrections from the momentum corrections by using the constraints provided by the elastic $ep \rightarrow ep$ scattering kinematics. Assumption 2 and 3 allow us to use the proton recoil angle and the beam energy to predict the polar and azimuthal angle of the elastically scattered electron.

In order to calculate the electron polar (θ_e) angle, we selected $ep \rightarrow e'p$ elastic events from the W cut ($0.7 < W < 1.05$ GeV) without any other PID cut except for proton polar angle cut ($\theta_p > 35^o$). After selection, we used the following relation (1). The electron polar angle (θ_e) can be calculated from the proton polar angle (θ_p) and beam energy (E_0) through 2-body kinematics. This means the calculated $(\theta_e)_{calc}$ can be represented as a function of E_0, θ_p ;

$$\theta_{ecal} = 2\ tan^{-1}\Big(\frac{m_p}{(E_0 + m_p)\ tan\theta_p}\Big) \tag{1}$$

The difference ($\delta\theta_e = \theta_{calc} - \theta_{meas}$) of the calculated and measured polar angles of electron was analyzed for all ϕ and θ angles. In order to do this, we divided polar angle from 13^o to 26^o in 1^o bins and selected elastically scatterd electron angle range. We looked at the distribution of $\delta\theta_e$ as a function of ϕ. The $\delta\theta_e$ can be represented by the following dunction ;

$$\begin{aligned}
\delta\theta_e &= \theta_{ecalc} - \theta_{emeas} = f(\theta_e, \phi_e, sec) && (2)\\
&= A(\theta_e, sec) * \phi_e^4 + B(\theta_e, sec) * \phi_e^3 + C(\theta_e, sec) * \phi_e^2 \\
&\quad + D(\theta_e, sec) * \phi_e + E(\theta_e, sec) && (3)\\
&= (\alpha^A{}_{sec} * \theta_e^2 + \beta^A{}_{sec} * \theta_e + \gamma^A{}_{sec}) * \phi_e^4 \\
&\quad + (\alpha^B{}_{sec} * \theta_e^2 + \beta^B{}_{sec} * \theta_e + \gamma^B{}_{sec}) * \phi_e^3 \\
&\quad + (\alpha^C{}_{sec} * \theta_e^2 + \beta^C{}_{sec} * \theta_e + \gamma^C{}_{sec}) * \phi_e^2
\end{aligned}$$

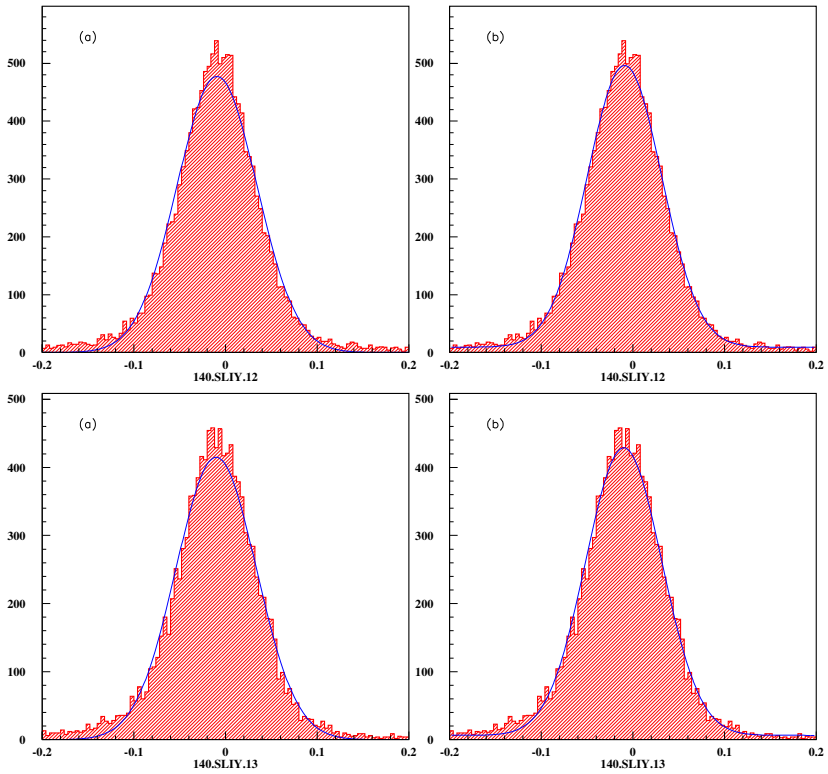

Figure 2: Fitting $\delta\theta_e$ vs. ϕ_e. At θ_e is $13^o < \theta_e < 14^o$ in sector 1 : Top and bottom plots are relate to different ϕ_e bin. Fits are with sigle Gaussian in (a), constant + Gaussian in (b).

$$+ (\alpha^D{}_{sec} * \theta_e^2 + \beta^D{}_{sec} * \theta_e + \gamma^D{}_{sec}) * \phi_e$$
$$+ (\alpha^E{}_{sec} * \theta_e^2 + \beta^E{}_{sec} * \theta_e + \gamma^E{}_{sec}) \quad (4)$$

where, $\alpha^A{}_{sec}, \beta^A{}_{sec}, \gamma^A{}_{sec}$ are the parameters of 4-th order term of ϕ and θ and the indecies A, B, C, D and E are related to the power of ϕ. The ϕ_e dependence of $\delta\theta_e$ was obtained by fitting a constant + Gaussian to the $\delta\theta_e$ distribution for each ϕ_e bin. The mean values of the fitted Gaussian are fitted to construct the correction function. The correction function contains 90 parameters and these parameters can describe $\delta\theta_e$. Figure 2 shows an example of fits to the azimuthal angle and polar angle for $13^o < \theta_e < 14^o$ in sector 1.

Figure 3 and 4 show the fitted $\delta\theta_e$ vs. ϕ_e in sector 1. Clearly, the measured

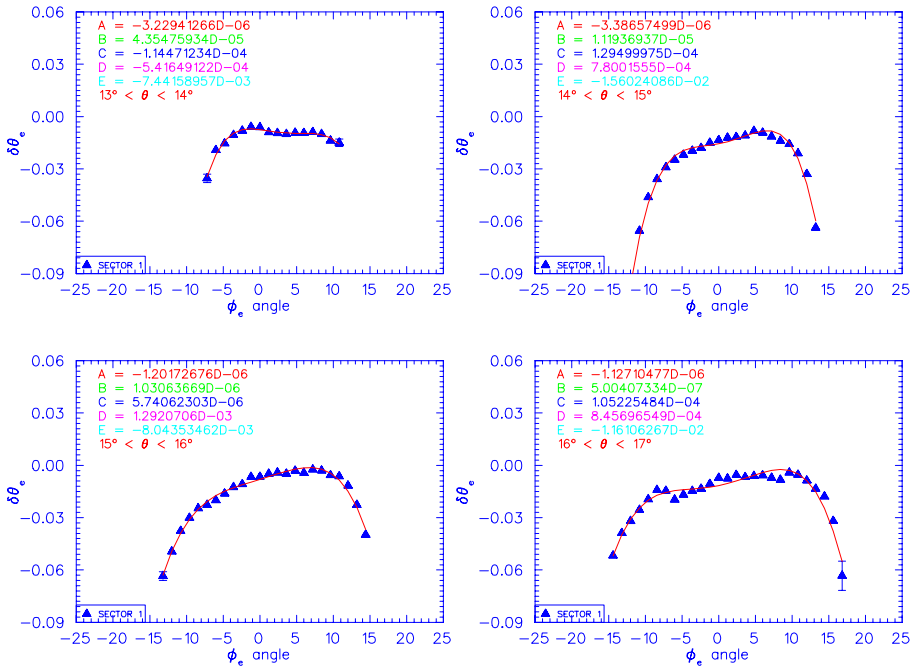

Figure 3: After proton angle cut ($\theta_p > 35^o$), the plot of the electron polar angle difference (as defined by $\delta\theta_e = \theta_{meas} - \theta_{calc}$) vs. ϕ_e for $13^o < \theta_e < 17^o$ in sector 1. Fit function is $f = A * \phi^4 + B * \phi^3 + C * \phi^2 + D * \phi + E$.

electron angles need to be corrected. However, the maximum correction is of the order of 1 mrad.

In order to describe the distributed data points, we used a 4-th order polynomial function. The main reason to using the high order polynomial function is that the very fowward polar angle region (between 13^o and 17^o) has a more complicated shape than the others. The curvatures are getting simpler and flatter with increasing polar angle.

However, there could be a problem at extreme angle regions of such a high order correction function was applied. To avoid this, we make cuts on the polar angular region.

Figure 5 shows the θ_e dependence of each of the five fit parameters (A,B,C,D,E). As the ϕ_e dependent fit parameters have different scale range, we mutiply the scale factor to each parameter in order to determine their

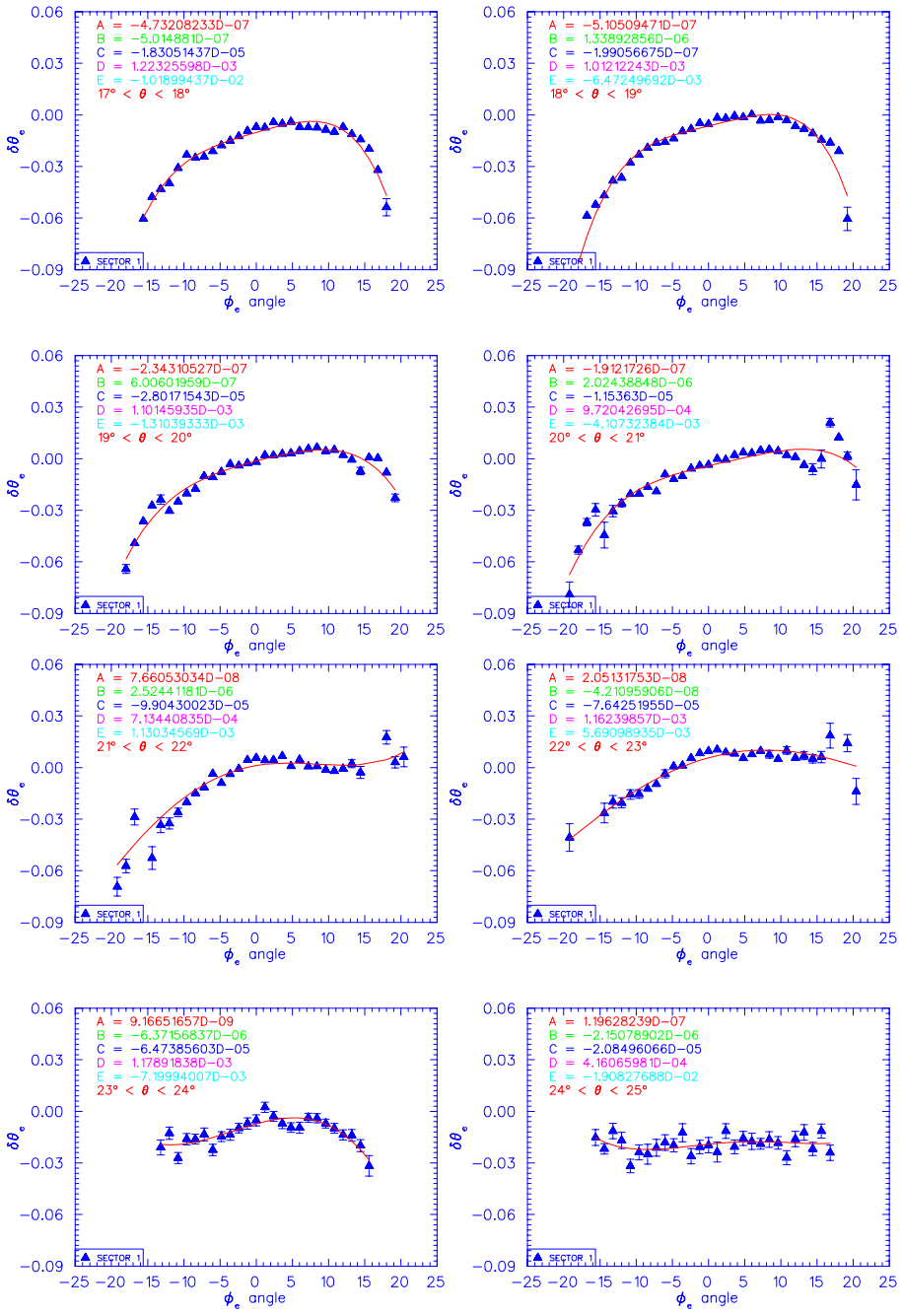

Figure 4: Electron polar angle difference vs. ϕ_e for $17^o < \theta_e < 25^o$ in sector 1. Each plot is related to each θ_e bin. Each plot is fitted by 4-th order polynomial function. Fit function is $f = A*\phi^4 + B*\phi^3 + C*\phi^2 + D*\phi + E$

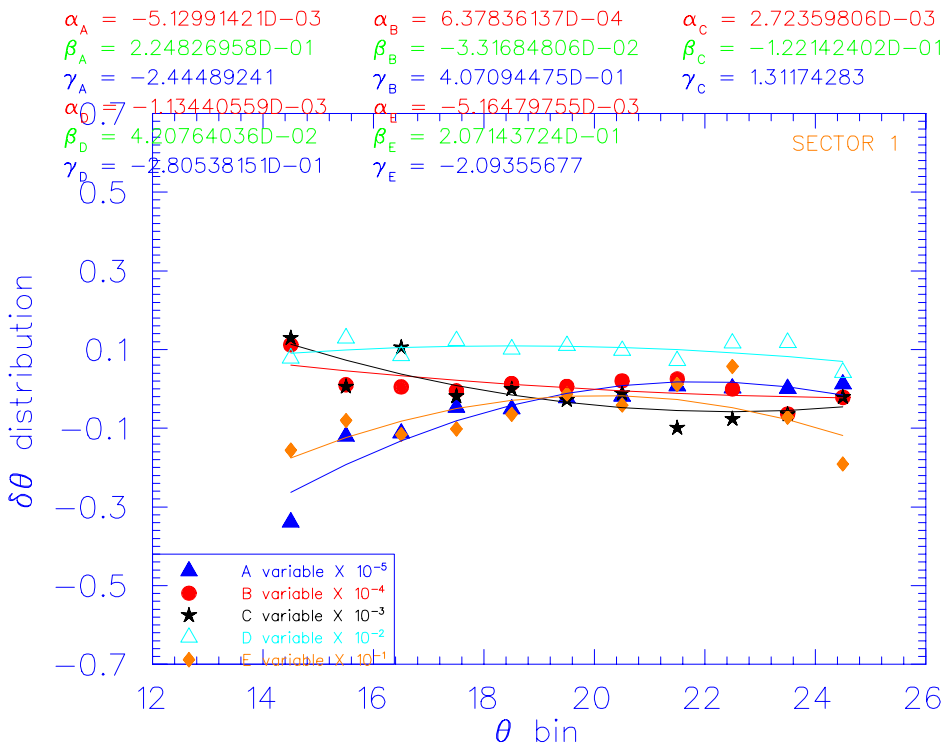

Figure 5: θ_e dependency of the ϕ_e fit parameters. Each data point ($-\star-$ $-\bullet-$ $-\diamond-$ $-\triangleleft-$) corresponds to the order of parameters in sector 1. To get the parameters, the fit function is used. $g_{A,B,C,D,E} = \alpha_{A,B,C,D,E} * \theta^2 + \beta_{A,B,C,D,E} * \theta + \gamma_{A,B,C,D,E}$. The indices (A,B,C,D,E) of function correspond to each fit parameters from Figure 3 and Figure 4

θ_e dependence. We then fit the θ_e distribution with a 2nd order polynomial function and obtain the three θ_e-dependent fit parameters ($\alpha_A, \beta_A, \gamma_A$ in each ϕ_e dependent fit parameter). Finally, we use those parameters to determine the constants for the electron scattering angle corrections.

3.2.2 Results of angle corrections

After determining the correlation between θ_e and ϕ_e, we constructed the correction function based on this relation. We measured the same quantities after applying angle corrections. Figure 6 and figure 7 show the resulting dependence. Since the angle corrections are small we do not see significant

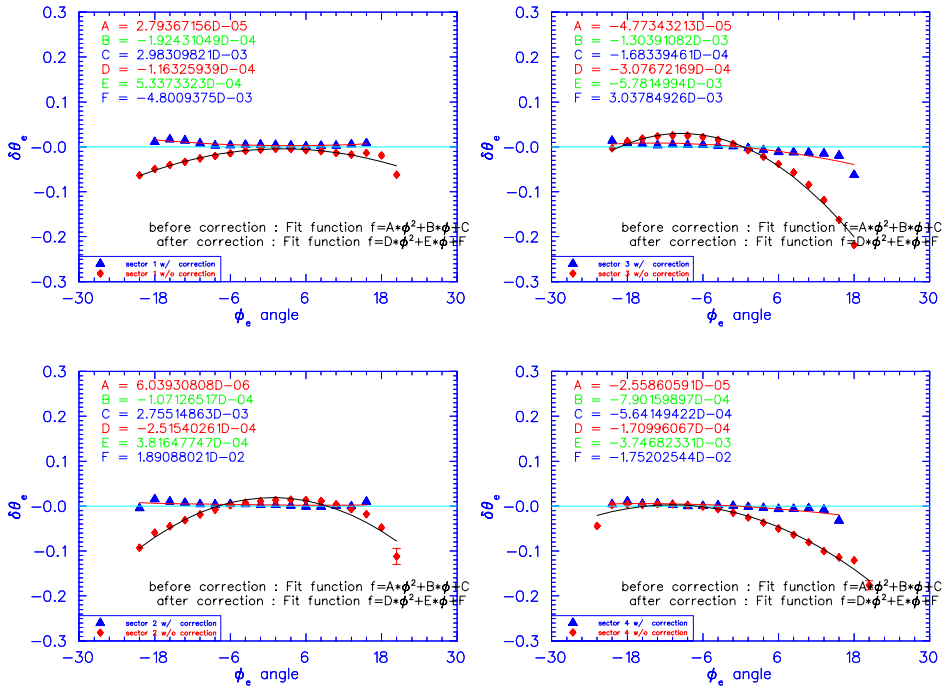

Figure 6: Comparison of $\delta\theta_e$ dependence on ϕ_e before (red diamond) and after (blue triangle) electron angle correction in Sector 1,2,3 and 4. All sectors show similar improvements.

improvement in Figure 8 with the electron angle corrections applied. The W is missing mass is little affected by the electron angle corrections. We conclude that the shift in the elastic peak is largely due to systematic shifts in the momentum reconstruction.

3.2.3 Effect of angle corrections on missing mass

By measuring the process $ep \rightarrow e'\pi^+X$ we can use the missing mass technique to calculate the neutron mass. Table 1 shows the missing mass of the neutron before and after electron angle corrections are applied in each sector. The shift is very small. The reason is that each sector contains the integrated events over all ϕ_e and θ_e. However, if we plot the missing mass versus $cos\theta_e$ as shown in Figure 9, we can recognize a very small difference.

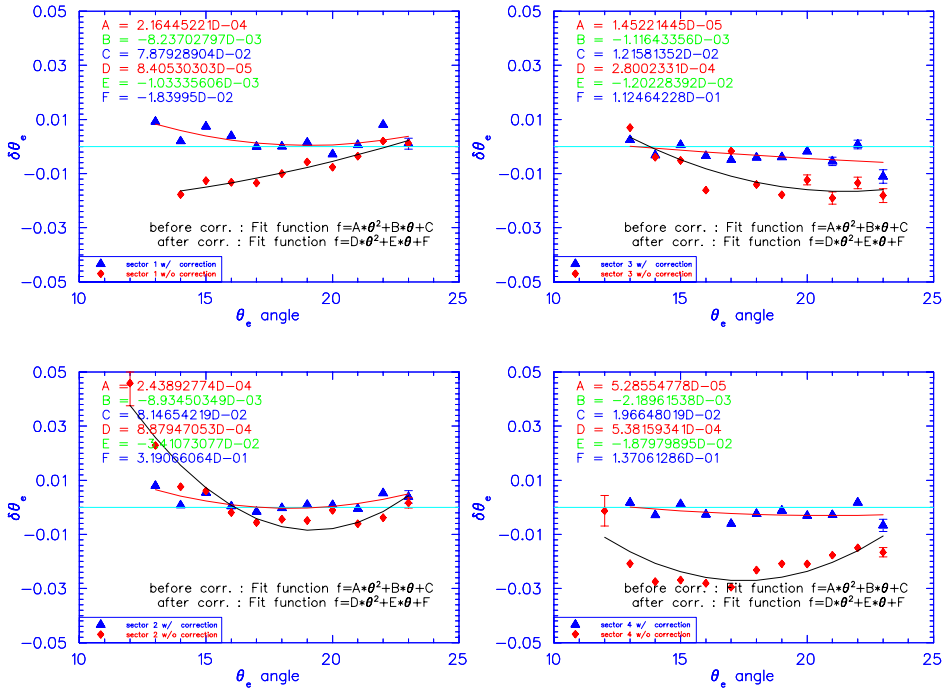

Figure 7: Comparison of $\delta\theta_e$ dependence on θ_e before (red diamond) and after (blue triangle) electron angle correction in Sector 1,2,3 and 4

SECTOR	Before mean	Correction sigma	After mean	Correction sigma
1	0.9550	0.2159E-01	0.9550	0.2159E-01
2	0.9518	0.2304E-01	0.9518	0.2305E-01
3	0.9503	0.2317E-01	0.9503	0.2317E-01
4	0.9539	0.2608E-01	0.9540	0.2610E-01
5	0.9398	0.2784E-01	0.9398	0.2784E-01
6	0.9463	0.2506E-01	0.9463	0.2505E-01

Table 1: The mean and width of missing mass neutron before and after applying the electron angle correction $[GeV/c^2]$

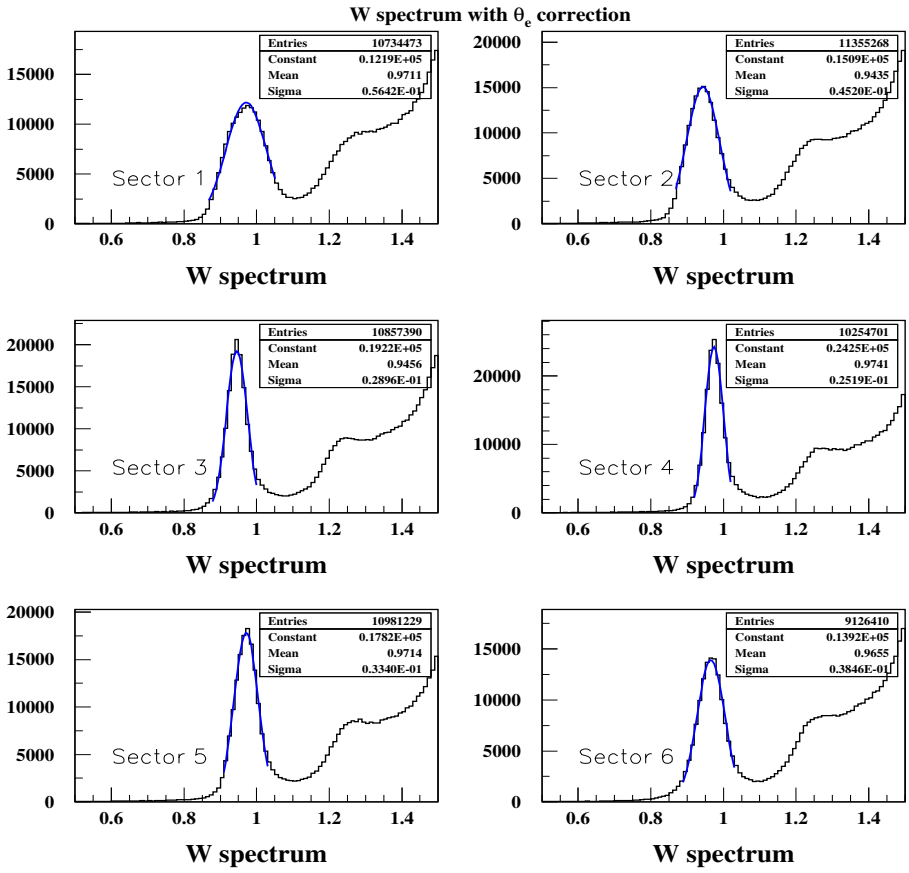

Figure 8: W spectrum with electron angle correction. From left top to right bottom, from sector 1 to 6

3.2.4 Conclusion from angle corrections

The effect of the electron angle correction on the neutron missing mass in each sector is very small. However, we can truly recognize the very small difference in the $cos\theta_e$ dependence before and after corrections are applied. The main reason for such a small electron angle effect is that the missing mass technique strongly depends on both electron momentum and hadron momentum which at this step have not been corrected for.

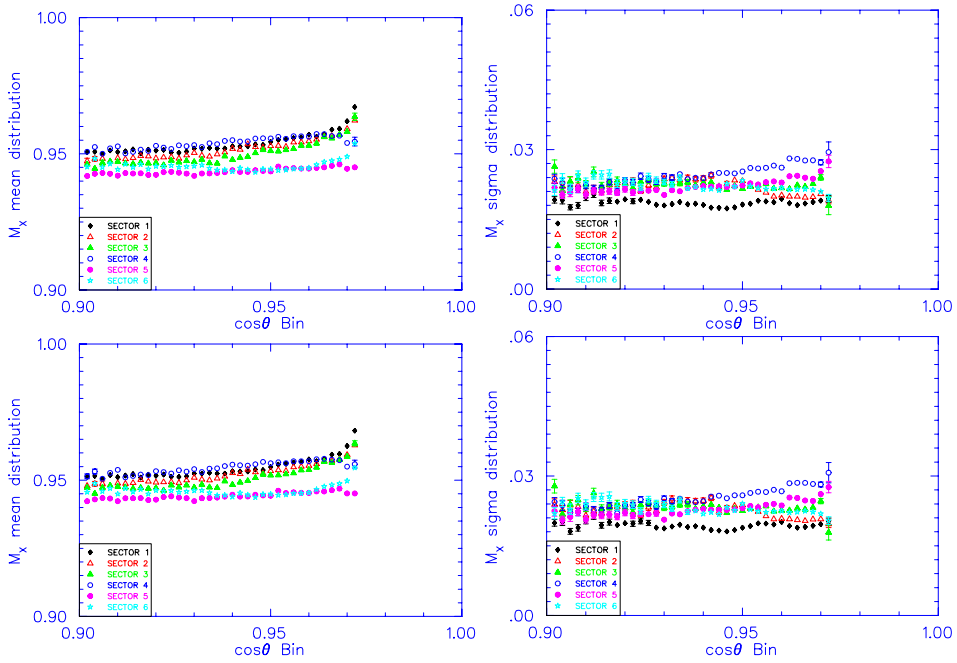

Figure 9: Missing mass of neutron (peak centroid (left) and width (right)) vs. $cos\theta_e$ before (top) and after(bottom) electron angle correction is applied.

3.3 Momentum corrections

3.3.1 Procedure

A systematic study of shifts in the elastic peak position in W and the neutron peak position in missing mass spectra have been performed by correcting the reconstructed electron angles. As mentioned in Sec.3.1, the shifts are due to the uncertainties in the torus field and misalignments in drift chamber. After corrections are applied, we can assume the measured electron angles are correct. We then calculate the exact electron momentum from true electron angles. The electron momentum correction is performed in two steps ; (1) Use the elastically scattered ep events to correct the electron momentum. (2) Verify the missing mass using $e'X$ and $e'\pi^+X$ kinematics.

To correct the electron momentum, two assumptions (1 and 3) as explained in Sec.3.1 are adopted. First, we use the beam energy $E_0 = 5.754$ GeV measured in Hall A and second, the electron polar angle is correct after angle correction. The angles are based on the assumption the proton polar angle is correct for angles greater than 35^o. Then, the elastic scattered electron candidates are chosen using a W cut in region $0.7 < W < 1.05$ GeV. We ignore a possible small shift of the peaks due to radiative effects.

The corrected electron momentum p_{ecalc} can be calculated from the known beam energy and the corrected electron polar angle. The calculated electron momentum has the correct value because we assumed that we had two pieces of exact information (beam energy E_0 and proton angle θ_p).

$$p_{ecalc} = \frac{E_0}{1 + 2\ E_0 sin^2\left(\frac{\theta_e}{2}\right)/m_p} \tag{5}$$

where, E_0 is the initial beam energy and m_p is the proton mass ($= 938.26$ MeV).

In general, there is no consensus on the expression that the correction function should have [4] . Therefore, the electron momentum correction should be a function of both momentum (p_e) and angles (θ_e and ϕ_e). And we can make separate correction function corresponding to each sector. The function is then ;

$$p_{corr} = f(p_{emeas}, \theta_e, \phi_e, sec) \tag{6}$$

where, p_{corr} is the 'real' value, and 'sec' indicates the sector. Since the main uncertainties are due to the distribution of the torus field and angles

mainly defined by DC geometry, we corrected electron angles and then used correctly measured angles, to determine the momentum values. We can write :

$$p_{e_{corr}} = p_{e_{meas}} \times g(\theta_e, \phi_e, sector) \tag{7}$$

$$\delta p_e \equiv p_{e_{corr}}/p_{e_{meas}} \tag{8}$$

We consider the correction function (g) as a scale factor which can be represented as a function of θ_e , ϕ_e and also depends on the specific sectors. We can write the relation (8) also in the following equations.

$$\delta p = p_{e_{corr}}/p_{e_{meas}} = g(\theta_e, \phi_e, sec) \tag{9}$$

$$= A'(\theta_e, sec) * \phi_e^3 + B'(\theta_e, sec) * \phi_e^2 + C'(\theta_e, sec) * \phi_e + D'(\theta_e, sec) \tag{10}$$

$$= (\alpha^{A'}{}_{sec} * \theta_e^2 + \beta^{A'}{}_{sec} * \theta_e + \gamma^{A'}{}_{sec}) * \phi_e^3 + (\alpha^{B'}{}_{sec} * \theta_e^2 + \beta^{B'}{}_{sec} * \theta_e + \gamma^{B'}{}_{sec}) * \phi_e^2 + (\alpha^{C'}{}_{sec} * \theta_e^2 + \beta^{C'}{}_{sec} * \theta_e + \gamma^{C'}{}_{sec}) * \phi_e + (\alpha^{D'}{}_{sec} * \theta_e^2 + \beta^{D'}{}_{sec} * \theta_e + \gamma^{D'}{}_{sec}) \tag{11}$$

where, $\alpha^{A'}{}_{sec}, \beta^{A'}{}_{sec}, \gamma^{A'}{}_{sec}$ are the parameters of 3-rd order term of ϕ_e and θ_e and the indicies A', B', C' and D' are related to the order of ϕ_e.

In the momentum case, the procedure is similar to the angle correction. The correction function is simply the ratio between the calculated modules of the electron momentum $p_{e_{calc}}$ and the measured $p_{e_{meas}}$ for each sector. The ratio contains 3-rd order ϕ_e term, 2nd order θ_e term and cross terms between θ_e and ϕ_e in each order term. Requiring $p_{e_{calc}} = p_{e_{meas}}$ we fit the ϕ_e and θ_e dependence for elastic events and extract the 72 correction parameters.

We used the same fit function (constant + Gaussian) as we have done for the angle corrections. We calculated and plotted the ratio of the calculated electron momentum and measured one for different ϕ_e and θ_e.

There is a significant correction in momentum needed after applying angle correction in ϕ_e and θ_e. Figure 11 and 12 contain the histograms of momentum difference versus ϕ in sector 1. Events detector edges and data points with large error at extreme ϕ_e values were ignored. The distribution

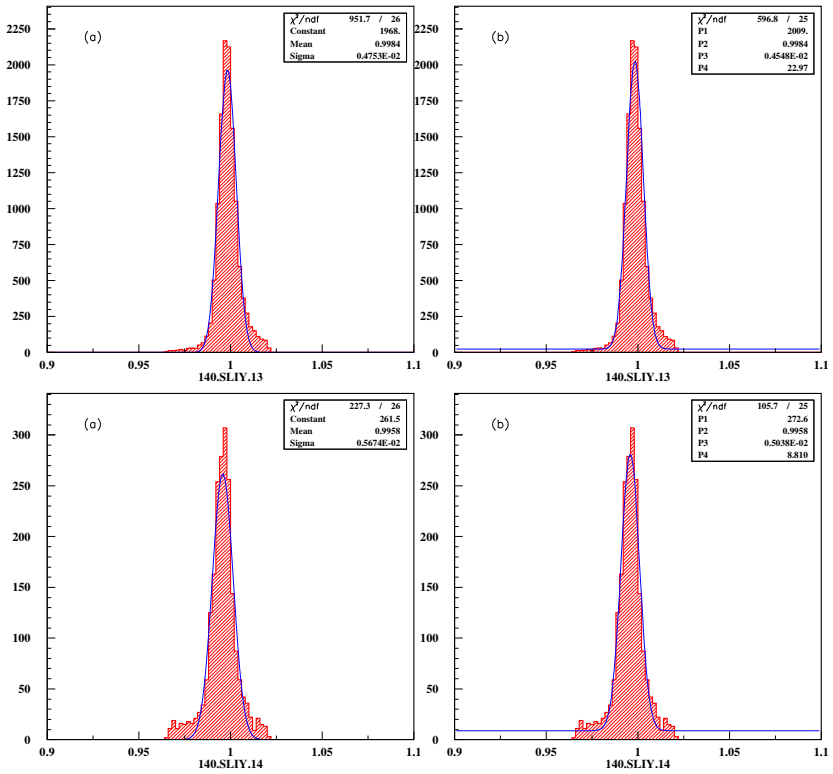

Figure 10: Fitting δp vs. ϕ_e slice bin in case of $13^o < \theta_e < 14^o$ in sector 1 : Top and bottom plots are relate to different ϕ_e bin. Fitting with sigle Gaussian in (a), constant + Gaussian in (b).

can be described by a 3-rd order polynomial function shown in Figure 11. There is no polar angle (θ_e) boundary to observe the electron momentum ratio. We can clearly see that the ratio of momentum moves toward 1.0 as electron polar angle increase (Figure 12 and 13).

We can extract four of the ϕ_e dependent fit parameters (A,B,C and D) in each θ_e bin as shown in Figure 14. We then fit these parameters with 2-nd order polynomial function. Figure 15 shows that the electron momentum difference (δp) approaches zero as the electron polar angle increases.

For polar angles greater than 35^o (this angle is approximated the angle which we assume for the proton polar angle range), we do not need mometum correction parameters.

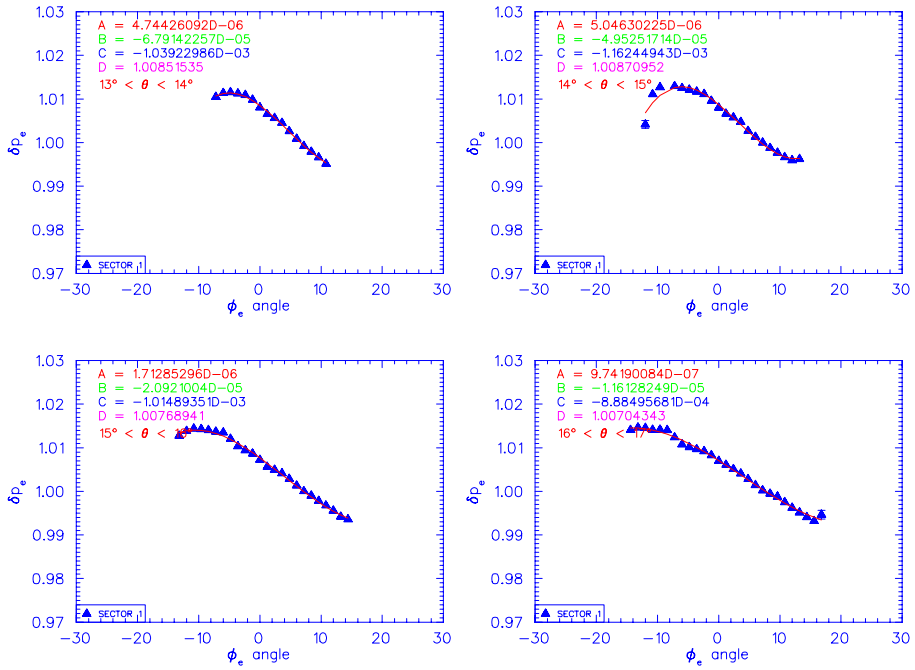

Figure 11: Electron momentum difference ($\delta p = p_{meas}/p_{calc}$) vs. ϕ_e in small polar angle range ($13^o < \theta_e < 17^o$). The fit is performed by 3-rd order of polynomial function $f = A * \phi^3 + B * \phi^2 + C * \phi + D$.

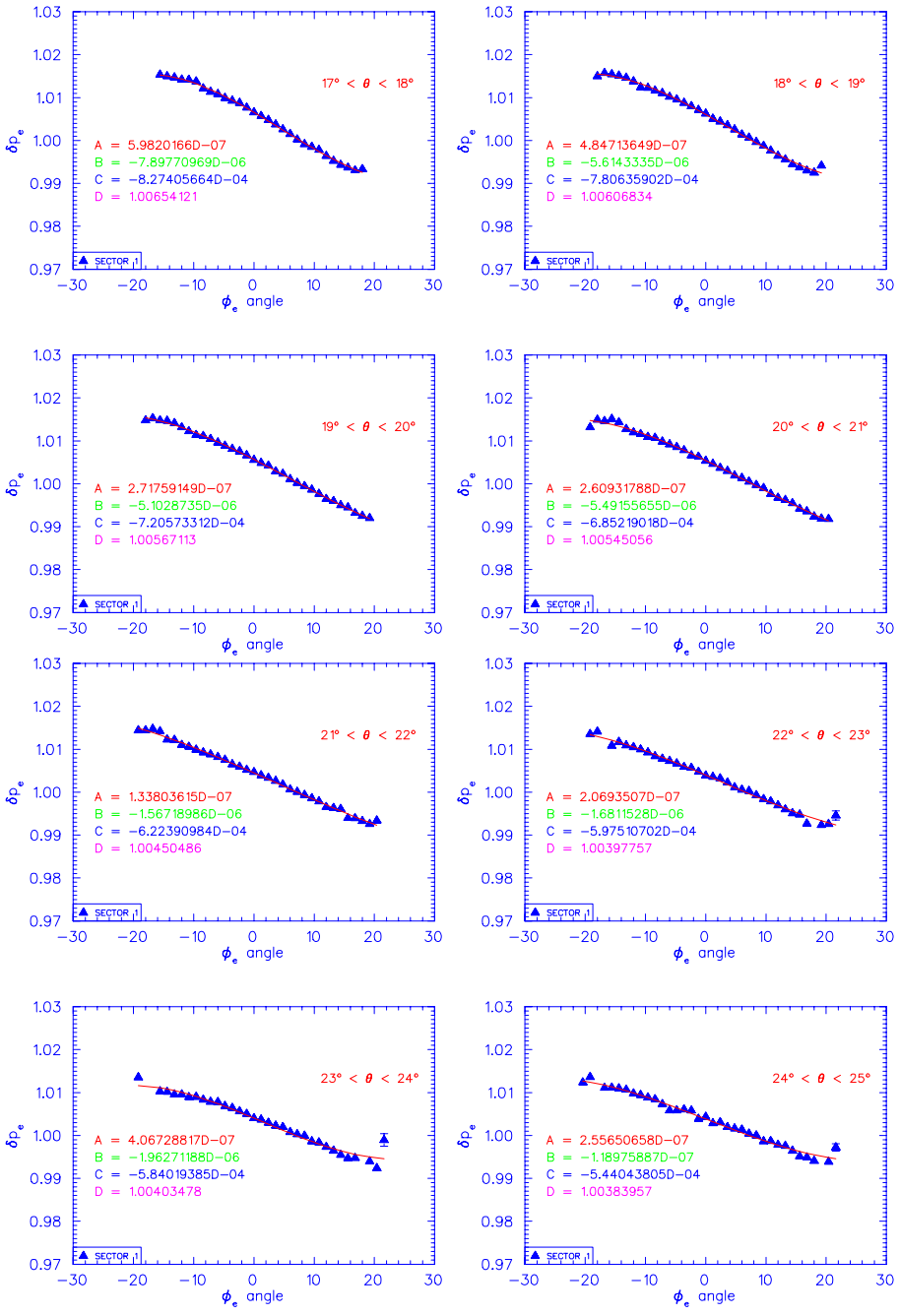

Figure 12: Electron momentum difference vs. ϕ_e in middle range ($17^o < \theta_e < 25^o$) of polar angle.

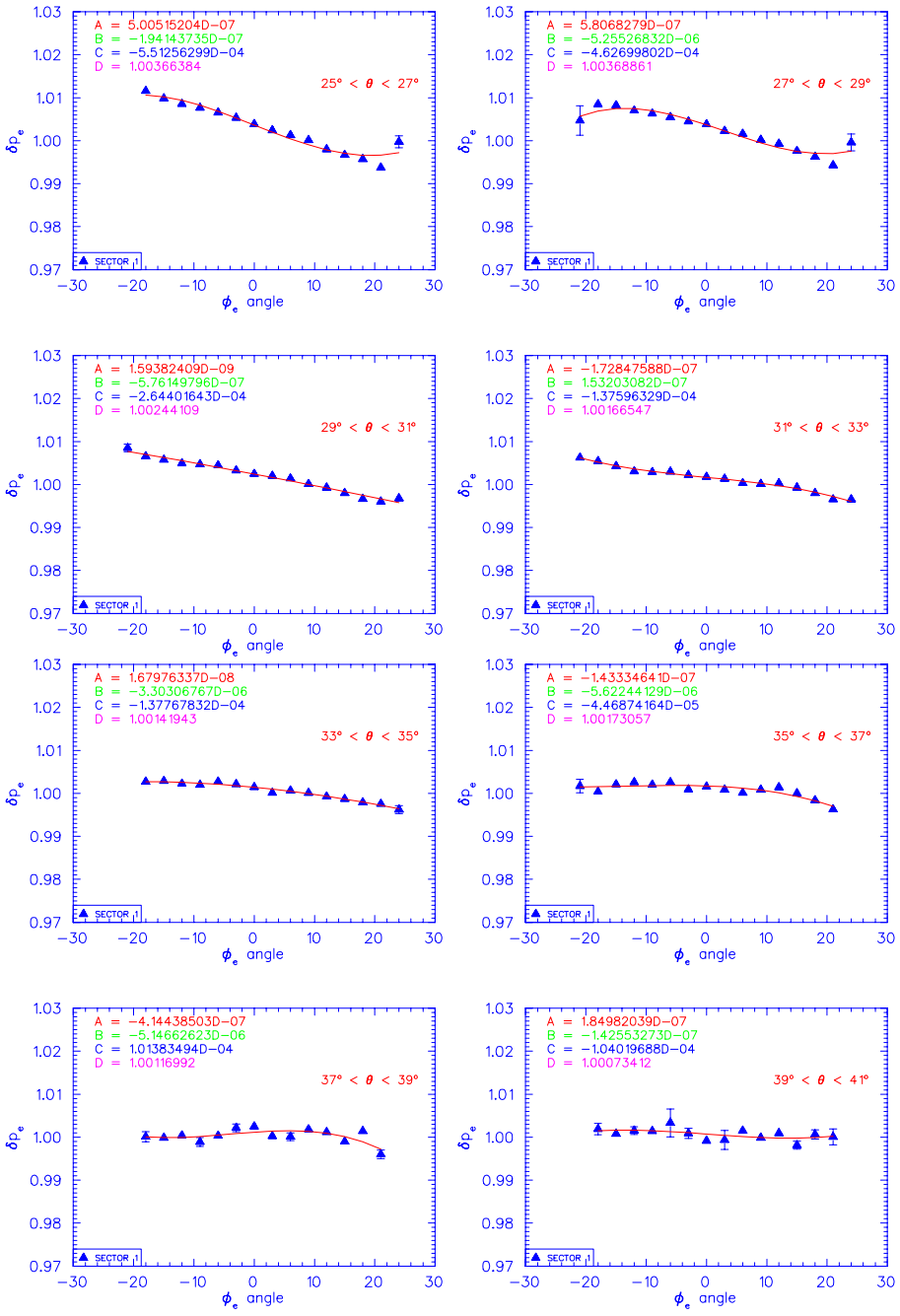

Figure 13: Electron momentum difference vs. ϕ_e in large range ($25^o < \theta_e < 41^o$) of polar angle. The bin size of polar angle is 2^o.

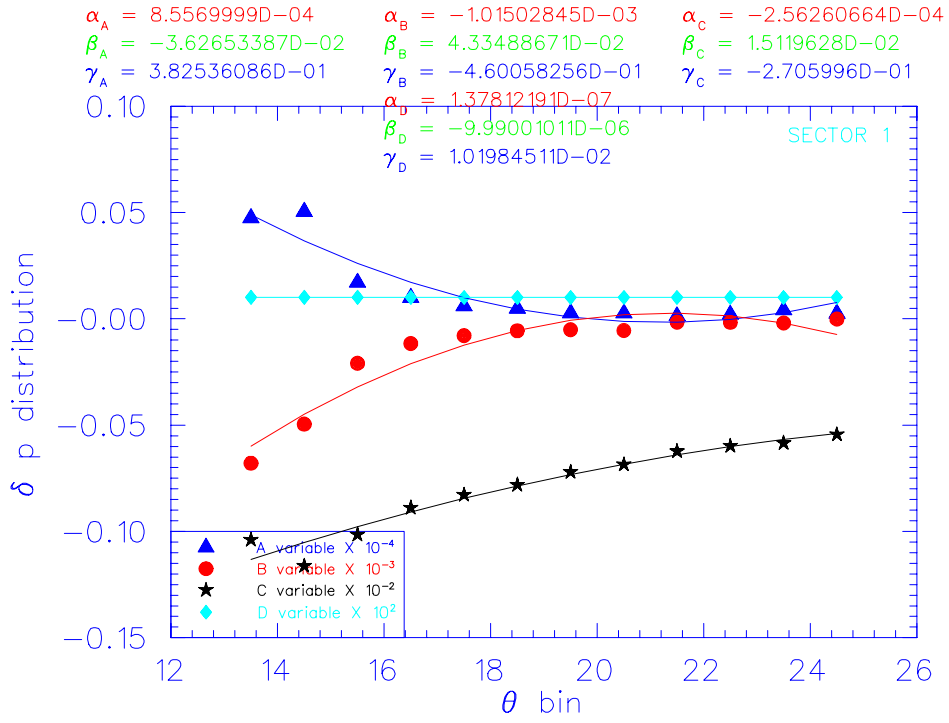

Figure 14: The ϕ_e fit parameters of δp versus θ around forward polar angle region. Each data point ($-\star-$ $-\bullet-$ $-\diamond-$ $-\triangleleft-$) corresponds to the order of paramters in sector 1. To get the parameters, the fit function is used. $g_{A,B,C,D,E} = \alpha_{A,B,C,D,E} * \theta^2 + \beta_{A,B,C,D,E} * \theta + \gamma_{A,B,C,D,E}$. The indices (A,B,C,D,E) of function correspond to each fit parameters from Figure11 and Figure12

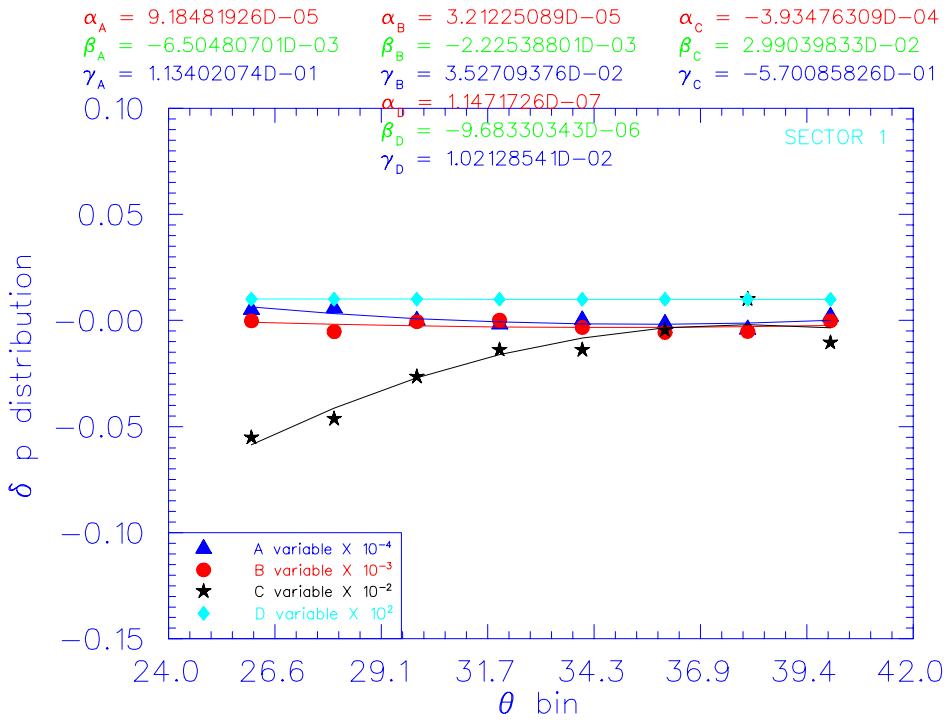

Figure 15: The ϕ_e fit parameters of δp versus θ around large polar angle region. All parameters converge zero over 35^o in sector 1. The indices (A,B,C,D,E) of function correspond to each fit parameters from Figure13

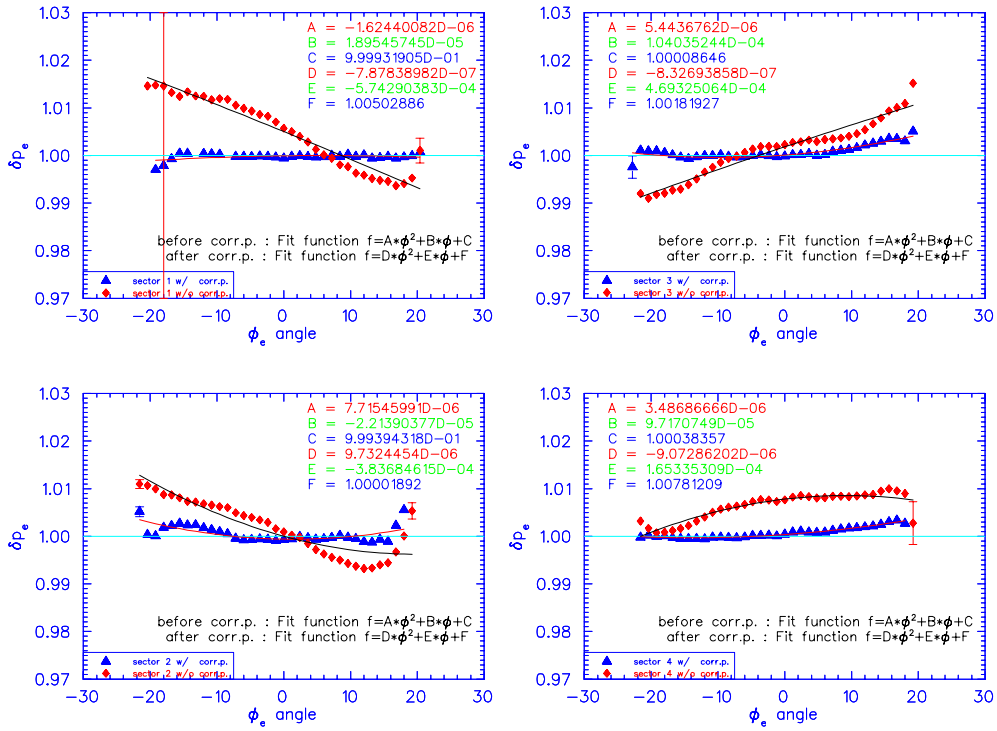

Figure 16: δp vs. ϕ_e before (red diamond) and after (blue triangle) electron angle and momentum correction in Sector 1,2,3 and 4

3.3.2 Electron momentum corrections from elastic scattering

After having determined the electron momentum correlation between θ_e and ϕ_e, we plot the same quantities (δp versus ϕ , θ) to help display details of the momentum correction function. Figure 16 and 17 show the improvement after applying momentum correction.

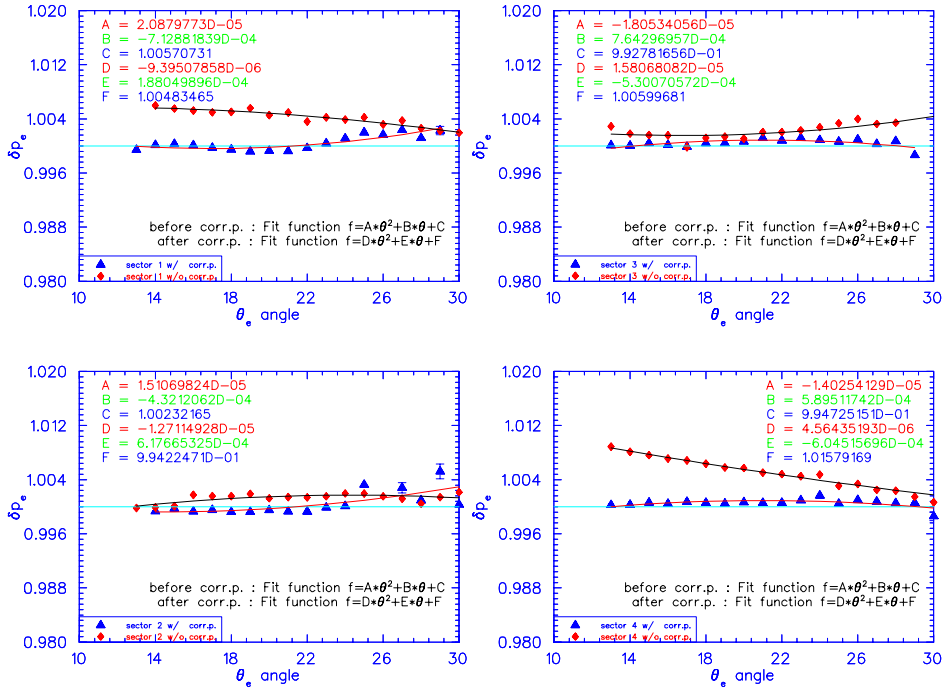

Figure 17: δp vs. θ_e before (red diamond) and after (blue triangle) electron angle and momentum correction in Sector 1,2,3 and 4

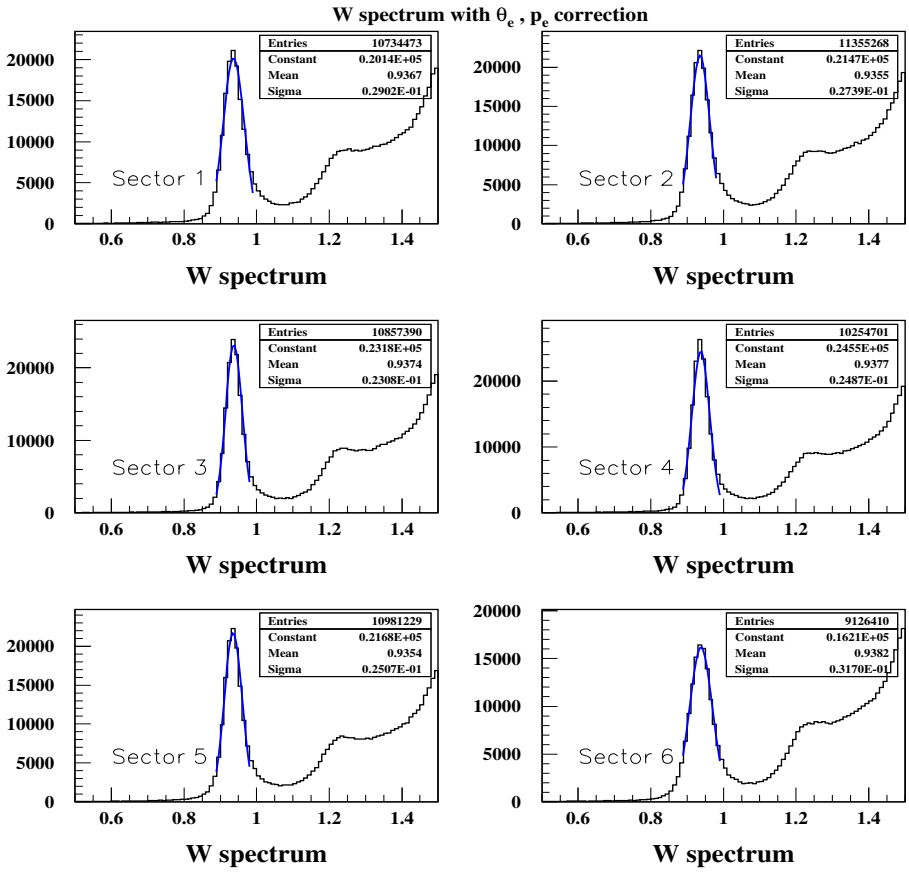

Figure 18: W spectrum after the correction for electron angle and momentum is applied

3.3.3 Corection results on elastic peak

Electron corrections are applied to 17% of E1-6 data set. Figure 18 shows the missing mass spectrum of $e'X$. Figure 18 indicates the proton mass with narrow resolution. The σ of elastic peak in each sector is less than 30 MeV. By comparing the resolution of Figures 1, 8 and 18, we can see that the resolution actually has improved, significantly. As shown in Figure 19, the electron corrections give significant improvement to mean and sigma of the elastic W distribution. The mean value of the missing mass $e'X$ is well aligned its the exact proton mass line and its sigma value has a maximum of less than 30 MeV.

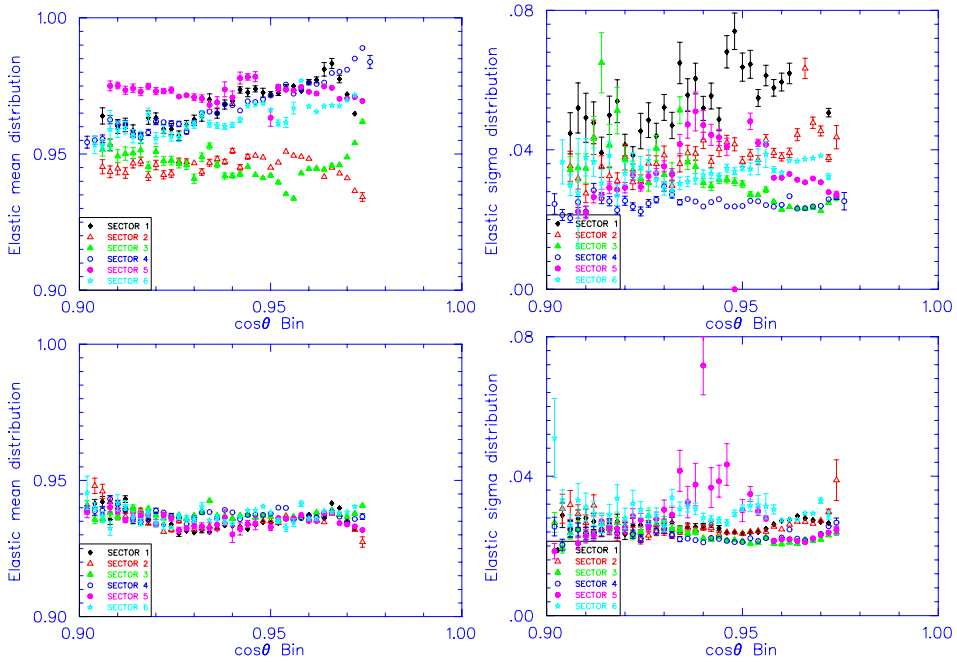

Figure 19: W spectrum versus $cos\theta$ without (top) and with (bottom) electron corrections.

3.4 Conclusions from electron angle and momentum corrections

We have observed the effect of electron corrections for angle and momentum. The angle corrections for electrons are too small to result in visible improvements in physics quantities. However, angle corrections are needed for the very forward polar angle region because of the possibility of misaligned drift chambers. It is clearly understandable when we look at the ϕ_e angle distribution through θ_e in Figure 3 and 4. We can see that there is an imrpovement on angle itself as shown in Figure 6 and Figure 7 . For the electron momentum, we can clearly see that the momentum correction functions give remarkable improvement.

3.5 Corrections for outbending trajectories

3.5.1 Effect of missing mass shifts in $ep \rightarrow e\pi^+n$ after electron corrections

The missing mass of $e'\pi^+X$ is well matched to the neutron mass (M_n = 939.55 MeV) with corrections for angle and momentum of the electron. All sectors show a well defined neutron peak with σ less than 20 MeV. Figure 21 shows the result of missing mass spectrum after applying electron angle and momentum correction. The effect of correction through θ_e in Figure 22 shows also remarkable improvement.

However, it is neccessary to correct the angles and momentum also for the positive charged particle, which could be different from the electron corrections due to the different trajectory. Looking at the Figure 20, it is clear that for $\theta_\pi < 40^o$ and $p_\pi > 2$ GeV. Some corrections are needed.

3.5.2 Angle corrections for outbending particles

The angle correction for outbending particles (especially in this case, π^+ particle) were performed using the same procedure as for electron angles. We assume that angle corrections do not depend on the particle charge.

3.5.3 Momentum corrections for outbending particles

To correct the momentum of outbending particles, we used the missing mass of the neutron in $e'\pi^+n$ final state. Events were selected that contained only

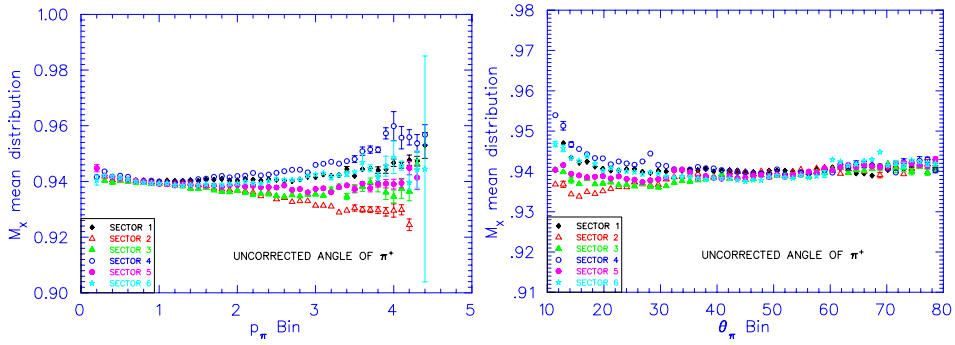

Figure 20: Plotting the missing mass of neutron versus the pion quantities (p_π, θ_π). We can still see the wrong neutron mass spectrum around high momentum of pion and low θ_π region even electron corrections applied.

one electron and one π^+. We applied a missing mass cut in the range from 0.85 and 0.99 GeV. The position of the missing mass peak of the neutron should be checked with quantities such as momentum and ϕ and θ angle of pion. Basically, the missing mass technique needs parameters of electron angles, momentum of electron, pion angles and momentum of pion. Figure 23, 24 show us the relation. As we have corrected the electron kinematics and pion angles, the missing mass of neutron is only dependent on the pion momentum. Now, we can plot the ratio (δM_X) of missing mass spectrum divided by the known neutron mass versus pion quantities (p_π, ϕ_π, θ_π). We can parameterize this ratio, and then extract the correction function for pion momentum. (See equation 12)

$$\begin{aligned} {M_X}^2 &= {E_n}^2 - {p_n}^2 \\ &= (E_0 + m_p - p_{e'} - E_\pi)^2 - ({p_{n_x}}^2 + {p_{n_y}}^2 + {p_{n_z}}^2) \\ &= \left(E_0 + m_p - p_{e'} - \sqrt{{p_\pi}^2 + {m_\pi}^2}\right)^2 \\ &\quad - \left((q_x - p_{\pi_x})^2 + (q_y - p_{\pi_y})^2 + (q_z - p_{\pi_z})^2\right) \end{aligned} \tag{12}$$

where, M_X is the neutron missing mass, E_n the neutron energy and p_n the 3-vector momentum. The first term in Equation 12 can be represented with the initial beam energy, proton mass, the scattered electron momentum and pion energy. The second term in Equation 12 can be re-written in terms

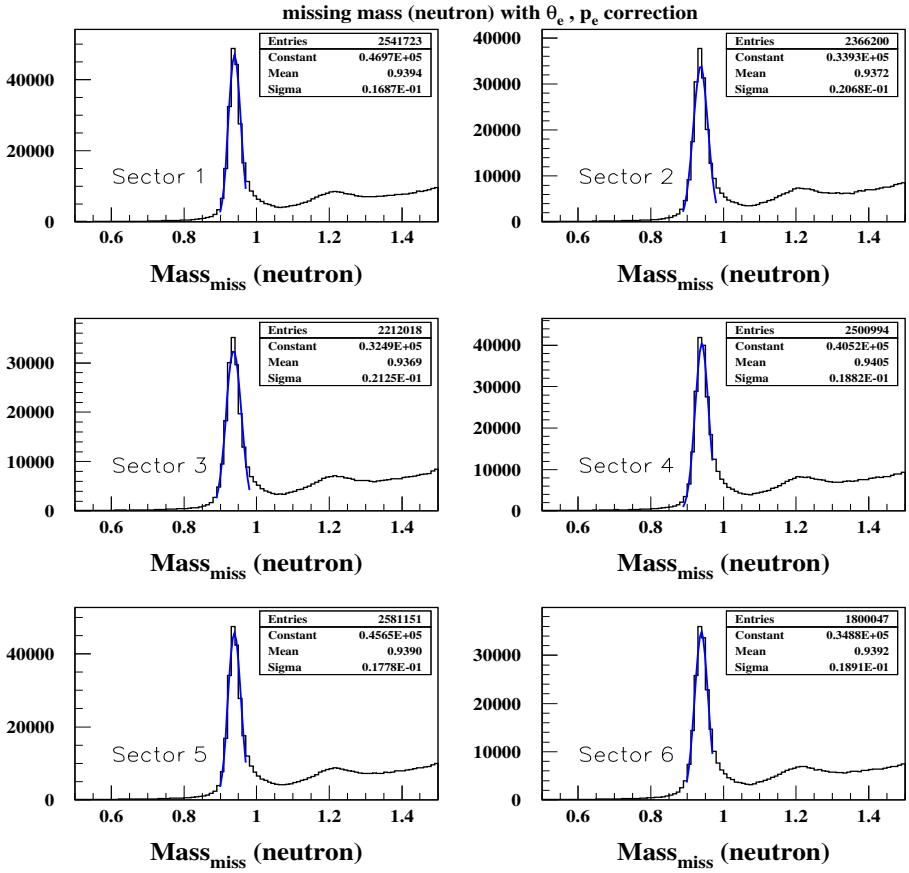

Figure 21: Missing mass spectrum of $e'\pi^+X$ after electron angle and momentum correction

of $\vec{q}$ and p_π. The variables in Equation 12 such as E_0, m_p, m_π are known constants, and some of them ($p_{e'}, q_x, q_y, q_z$) are the reliable values because of the already applied electron corrections. Therefore, the missing mass of the neutron should only depend on the pion momentum. The ratio of the measured missing mass of neutron and the known neutron mass can be represented as a function of θ_π, ϕ_π and sector as in Equation 13. We plot the δM_X through the ϕ_π and θ_π angles and extract the correction function by fitting all ϕ_π and θ_π cases. Figures 23, 24 and 25 show this ratio versus ϕ_π. As we can see from Figure 23 and 24, the small pion angle range (especially, $10^o < \theta_\pi < 24^o$) has a distorted distribution of ratio.

$$\delta M_X \quad = \quad M_{X\,meas}/M_{X\,value} = h(\theta_\pi, \phi_\pi, sec) \tag{13}$$

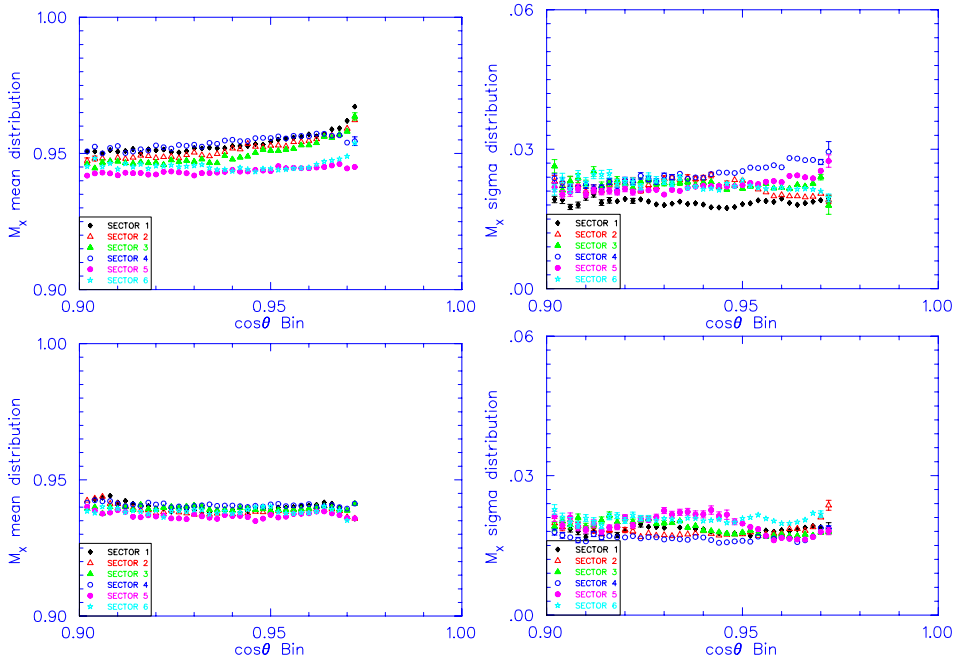

Figure 22: Missing mass of neutron versus $cos\theta$ without (top) and with (bottom) electron kinematic corrections. After applying the electron angle and momentum correction, the uncorrected missing mass of neutron (top) is significantly improved as a result (bottom).

$$
\begin{aligned}
&= A_h(\theta_\pi, sec) * {\phi_\pi}^4 + B_h(\theta_\pi, sec) * {\phi_\pi}^3 + C_h(\theta_\pi, sec) * {\phi_\pi}^2 \\
&\quad + D_h(\theta_\pi, sec) * \phi_\pi + E(\theta_\pi, sec) \qquad (14) \\
&= (\alpha^A_{h\,sec} * \theta_\pi^2 + \beta^A_{h\,sec} * \theta_\pi + \gamma^A_{h\,sec}) * \phi_\pi^4 \\
&\quad + (\alpha^B_{h\,sec} * \theta_\pi^2 + \beta^B_{h\,sec} * \theta_\pi + \gamma^B_{h\,sec}) * \phi_\pi^3 \\
&\quad + (\alpha^C_{h\,sec} * \theta_\pi^2 + \beta^C_{h\,sec} * \theta_\pi + \gamma^C_{h\,sec}) * \phi_\pi^2 \\
&\quad + (\alpha^D_{h\,sec} * \theta_\pi^2 + \beta^D_{h\,sec} * \theta_\pi + \gamma^D_{h\,sec}) * \phi_\pi \\
&\quad + (\alpha^E_{h\,sec} * \theta_\pi^2 + \beta^E_{h\,sec} * \theta_\pi + \gamma^E_{h\,sec}) \qquad (15)
\end{aligned}
$$

where, ${\alpha^{A_h}}_{sec}, {\beta^{A_h}}_{sec}, {\gamma^{A_h}}_{sec}$ are the parameters of 4-th order term of relation between pion angles (ϕ_π, θ_π) and missing mass neutron. And the indicies A_h, B_h, C_h and D_h are related to the order of ϕ.

Therefore, we decide that we apply the pion momentum correction to specific region only as the pion momentum correction are needed only in the high momentum region ($p_\pi > 2$ GeV), corresponds to small pion polar angle ($\theta_\pi < 40^o$). We used the final fit parameters in Figure 25 for correction. Figure 26 shows the final result for the missing mass spectrum after all corrections are applied.

3.6 Tests using other reactions

We have tested both angles and momentum corrections of the electron and positive pion also in $e'pX$ reaction channel. Especially, this reaction channel has three missing mass distribution ; π^0, η and ω. The Figures 27 and 28 show that the correction functions work also in the $e'pX$ reaction. All sectors have quite improved spectra with peak positions close to the known particle masses and quite improved good resolution. We can see the significant improvement of mean and width of π^0, η and ω from results of the $ep \rightarrow e'pX$ and neutron from $ep \rightarrow e'\pi^+X$ in Table 2.

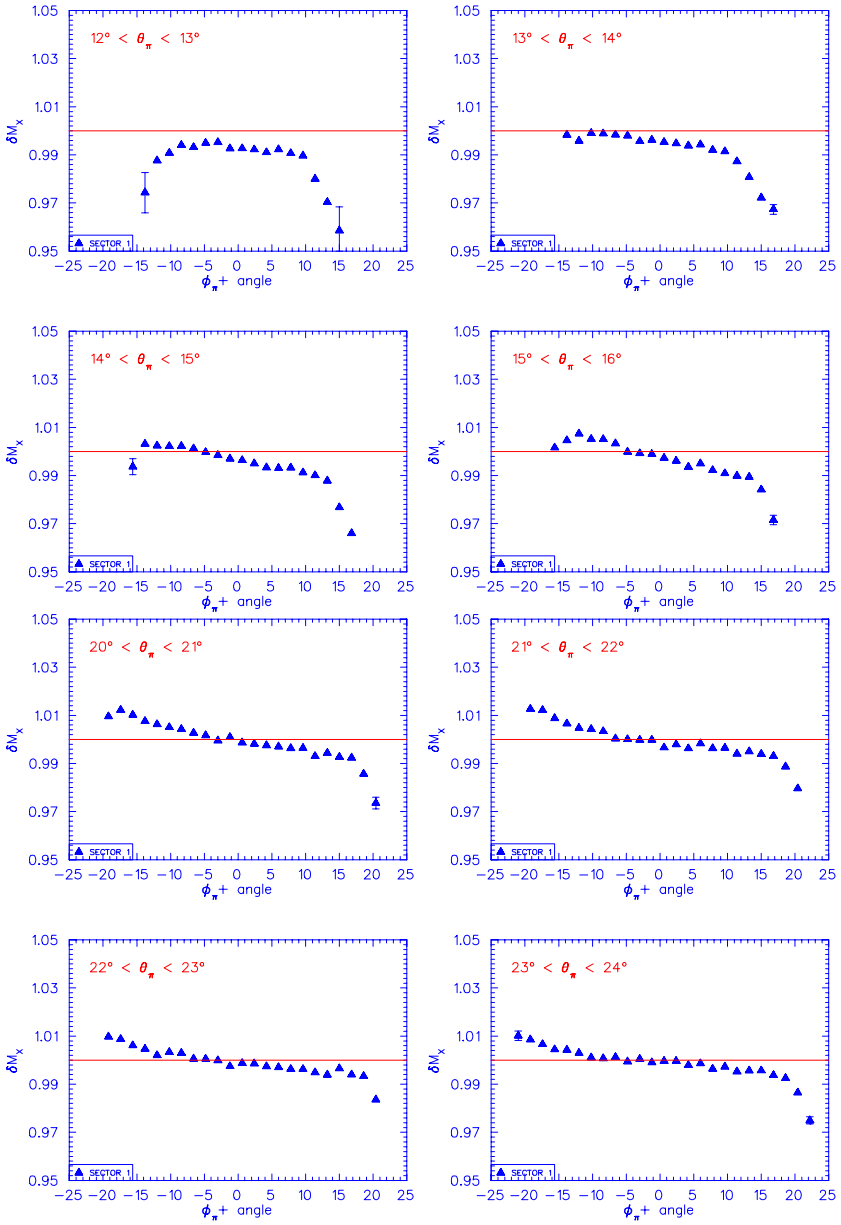

Figure 23: The ratio between measured missing mass of the neutron and known neutron mass versus ϕ_π through forward ($12^o < \theta_\pi < 16^o$ and $20^o < \theta_\pi < 24^o$) angle ranges.

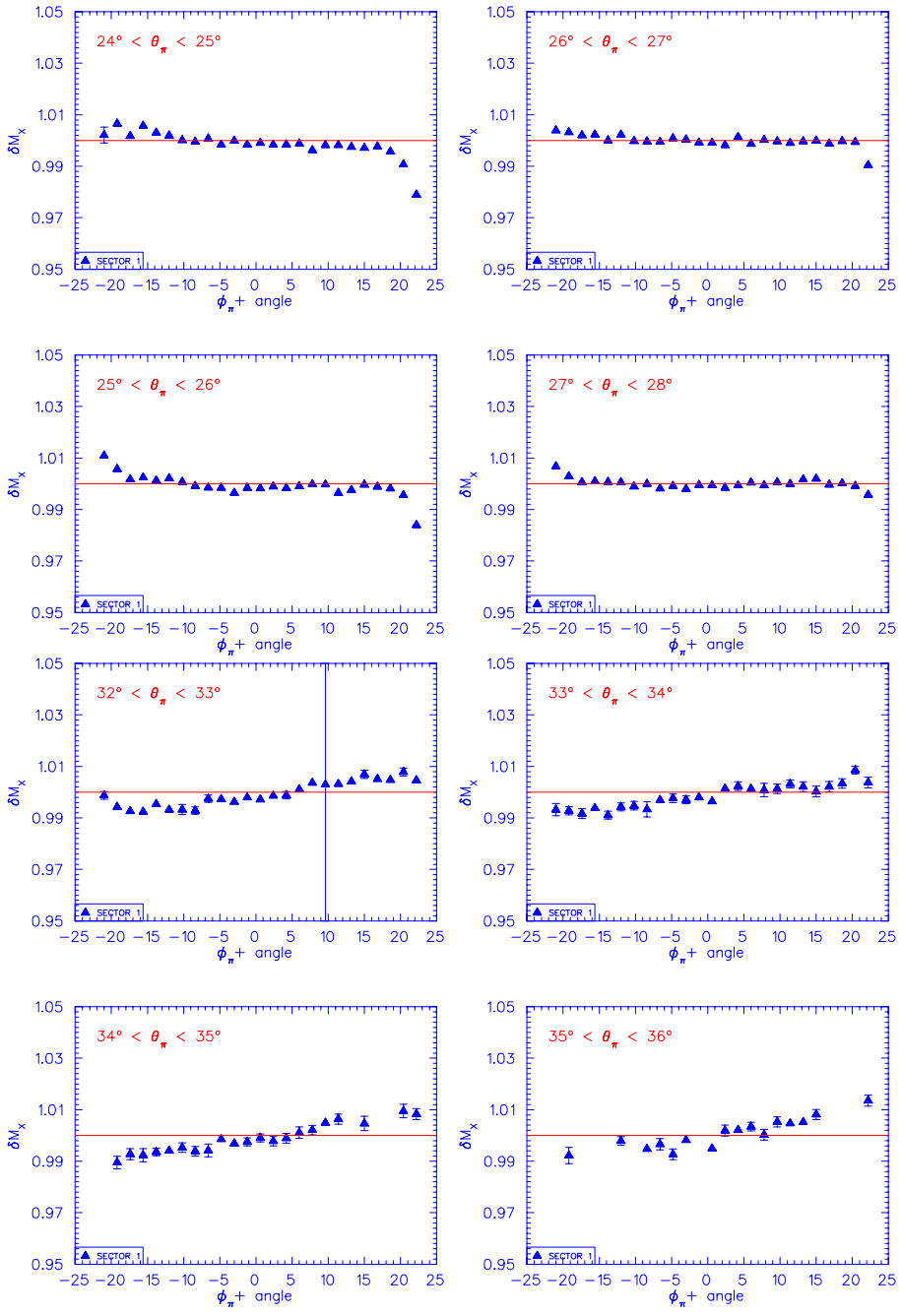

Figure 24: The ratio (δM_X) of measured neutron missing mass and known neutron mass vs. ϕ_π through large ($24^o < \theta_\pi < 28^o$ and $32^o < \theta_\pi < 36^o$) angle ranges.

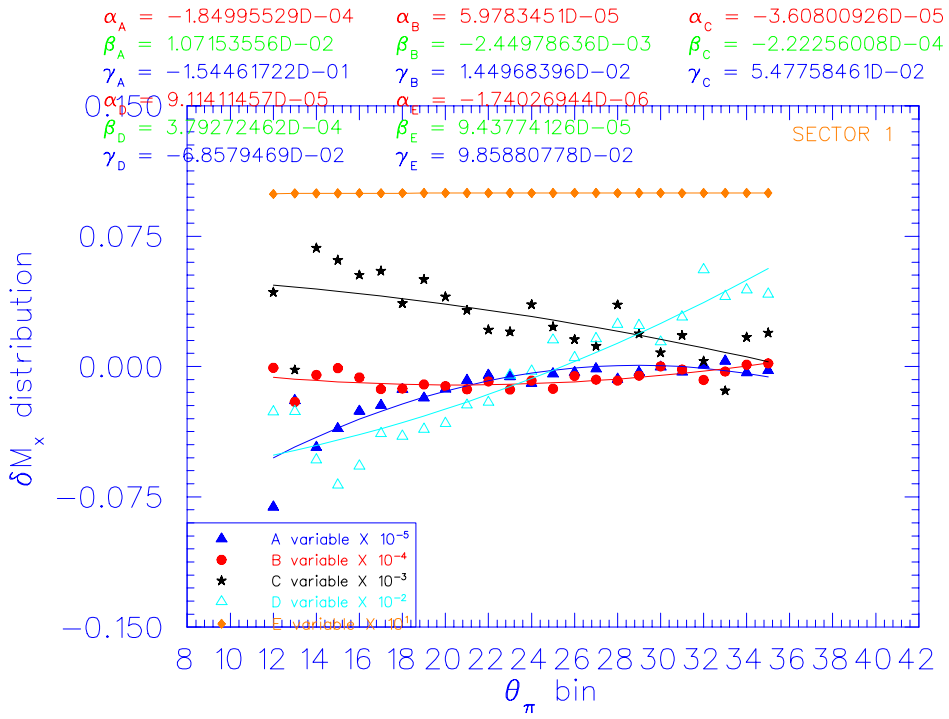

Figure 25: δM_X vs. θ_π. Each data point ($-\star-$ $-\bullet-$ $-\diamond-$ $-\triangleleft-$) corresponds to the order of paramters in sector 1. To get the parameters, the fit function $h_{A,B,C,D,E} = \alpha^h{}_{A,B,C,D,E} * \theta^2 + \beta^h{}_{A,B,C,D,E} * \theta + \gamma^h{}_{A,B,C,D,E}$ is used. The indices (A,B,C,D,E) correspond to the fit parameters in Figure 23 and Figure 24

MMX	PDG value mean	Before mean	Correction sigma	After mean	Correction sigma
π^0	0.13498	0.1586	0.4667E-01	0.1360	0.4093E-01
η	0.54730	0.5601	0.1535E-01	0.5467	0.1321E-01
ω	0.78257	0.7871	0.1838E-01	0.7806	0.1690E-01
n	0.93956	0.9495	0.2446E-01	0.9391	0.1831E-01

Table 2: The mean and width of missing mass of $e'pX$ and $e'\pi^+X$ before and after applying the kinematic corrections

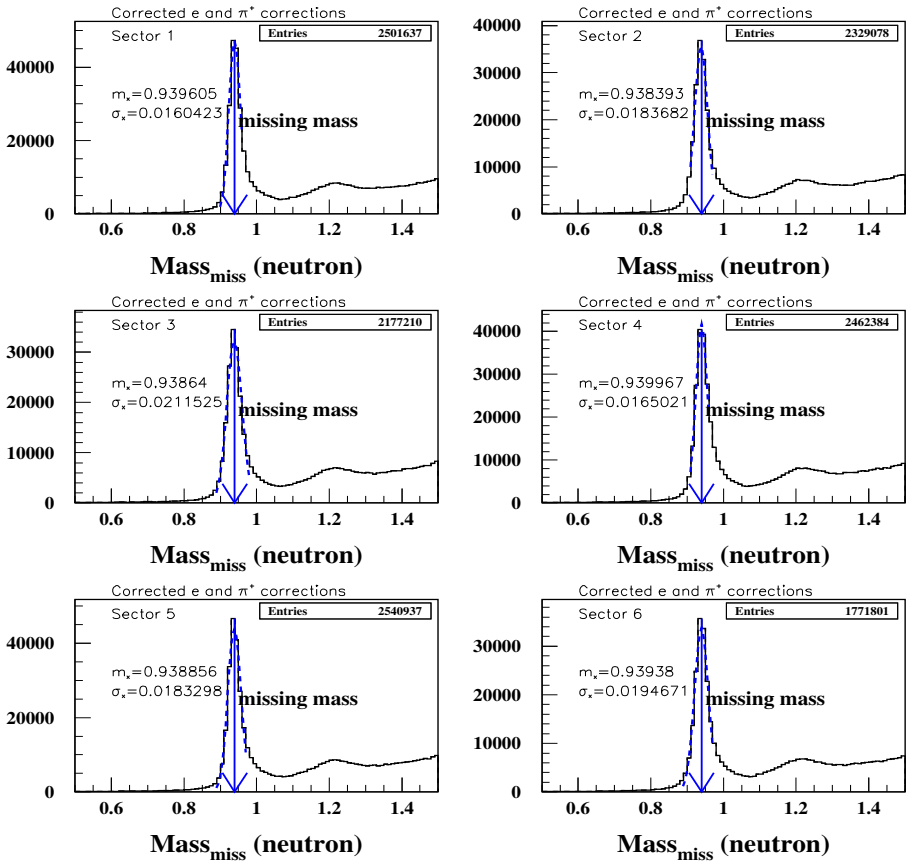

Figure 26: The missing mass of neutron after all corrections have been applied. From left top to right bottom, from sector 1 to 6

4 Conclusions

We have studied kinematic corretions for the $e'\pi^+n$ final state. We performed kinematic correction by observing the invariant mass (W, proton) and missing mass (M_X) spectra and developed an explicite polynomial parametrizations for the corrections. The quatities depend on both angle and momenta of the electron and the pion, respectively.

We find that angle corrections have very small effects on the W, M_X variables, while momentum corrections have much more important effects. Both the peak positions for the predictive and searched missing mass and their respective widths are significantly improved after the corrections are applied.

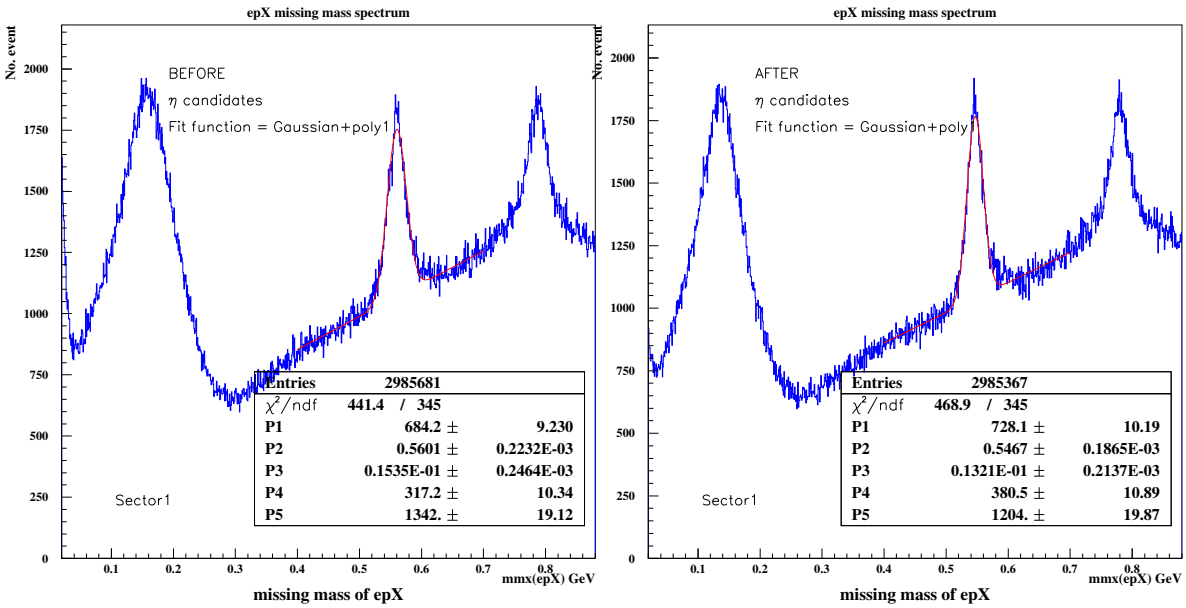

Figure 27: Missing mass spectrum of $e'pX$ (η) in sector 1

References

[1] V.D. Burkert, CALCOM presentation, www.jlab.org/Hall-B/equipment/technical/calcom/calcom-aug-21.txt.

[2] L.C. Smith, private communications.

[3] V. Koubarovski, private communications.

[4] D. Protopopeseu, F. W. Hersman, M. Holtrop, S. Stepanyan, "Electron Momentum Corrections for CLAS at 4.4 GeV", CLAS-NOTE 2001-008, May 8, 2001.

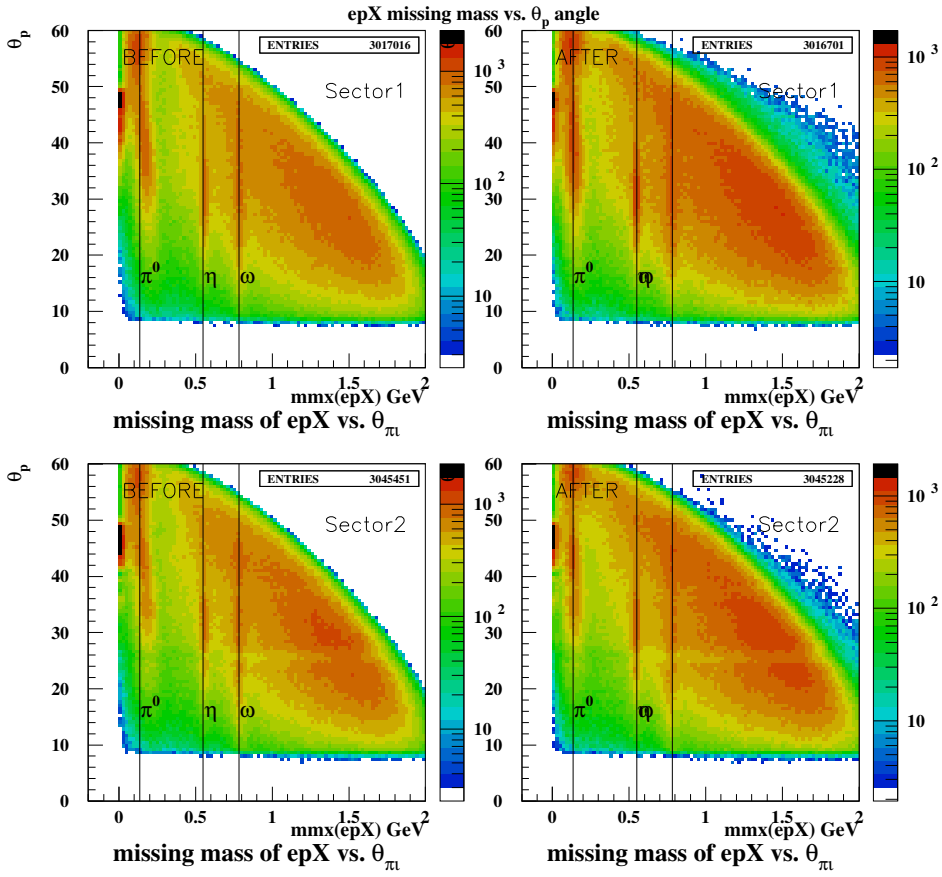

Figure 28: Missing mass of $e'pX$ vs. proton polar angle (θ_p) in sector 1,2